J. Fluid Mech. (2006), *vol.* 565, *pp.* 115–134. © 2006 Cambridge University Press
doi:10.1017/S0022112006001856 Printed in the United Kingdom

Ekman layers near wavy boundaries

By D. GÉRARD-VARET[1] AND E. DORMY[2,3]

[1]DMA/CNRS, Ecole Normale Supérieure, 45, rue d'Ulm, 75230 Paris Cedex 05, France

[2]LPS/CNRS, Département de Physique, Ecole Normale Supérieure, 24, rue Lhomond, 75231 Paris Cedex 05, France

[3]IPGP, 4 place Jussieu, 75252 Paris Cedex 05, France

(Received 17 September 2005 and in revised form 3 April 2006)

We investigate the effect of boundary roughness on the dynamical properties of the flow in laminar Ekman boundary layers. The study considers wavy boundaries having both horizontal wavelength and vertical extent comparable in size with the boundary layer width. In the case of flat boundaries, Ekman layers are known to be active, i.e. to affect significantly the dynamics of the mainstream flow. We show how the layer modelling needs to be modified to account for such wavy boundaries. In particular, nonlinear terms enter the laminar description. This model can be linearized in the limit of small Reynolds numbers. The resulting equations are studied using both asymptotic expansions and full numerical simulations. We find that small-scale roughness significantly alters energy dissipation in the boundary layer. This can result in either a reduction or an increase of dissipation, depending on, in particular, the orientation of the mainstream flow with respect to boundary modulation. Agreement is obtained between theoretical and computational results.

1. Introduction

Ekman layers (Ekman 1905) form when fluid flow strongly influenced by rotation meets a boundary which is not parallel to the axis of rotation. Such layers are ubiquitous in geophysical fluid dynamics: at the top of the ocean (where they were originally discovered), at the bottom of the ocean, at the base of the atmosphere, and at the top of the Earth's liquid core. A similar structure develops at the base of the solar convection zone (Ponty, Gilbert & Soward 2001). The description of Ekman layers next to flat horizontal or slanted boundaries is well established in terms of asymptotic expansions (e.g. Greenspan 1968). Yet in most of the relevant situations the boundary is not flat. Provided the typical wavelength of the boundary profile remains long compared to the boundary layer thickness, its effect can be taken into account under the quasi-geostrophic approximation (see Pedlosky 1979, and recent developments by Vanneste 2000). If the amplitude of the boundary profile significantly exceeds the boundary layer width, it directly affects the mainstream flow by altering geostrophic contours (Bell & Soward 1996). The case of rough boundary for which neither the wavelength nor the amplitude is large compared to the boundary layer size remains to be addressed. This occurs quite often at the bottom of the ocean (e.g. Kunze & Llewellyn Smith 2004) or at the top of the Earth's outer core (e.g. Narteau *et al.* 2001) where the bounding surface can be very rough and wavy at a scale comparable both in amplitude and in wavelength with that of the boundary layer itself. The investigation of such a configuration constitutes the object of the present research.

https://doi.org/10.1017/S0022112006001856 Published online by Cambridge University Press

2. Model setup and governing equations

2.1. *Dimensional equations*

We consider a very simplified model for one of the geophysical flows mentioned above. A local Cartesian approximation is adopted with coordinates (X, Y, Z). For simplicity, we assume that the rotational axis is aligned in the direction of the Z-coordinate.

We investigate flows between an upper and a lower boundary. For simplicity, the upper boundary is considered flat, so that roughness effects will only appear adjacent to the lower boundary. Moreover, the upper boundary may be neglected, either by considering stress-free boundary conditions, or through a proper choice of the pressure gradient (e.g. Ponty *et al.* 2001), so that, in our model, an Ekman layer only develops near the wavy lower boundary.

Throughout this paper, the fluid is assumed to be incompressible, rotating at constant angular velocity Ω, with constant rotation vector along the vertical axis: $z = (0, 0, 1)$. In the rotating frame of reference, the Navier–Stokes equations take the standard form

$$\left.\begin{aligned} \partial_{t^*}\boldsymbol{U}^* + \boldsymbol{U}^*\cdot\nabla^*\boldsymbol{U}^* + \frac{\nabla^*\pi^*}{\rho^*} + 2\Omega z\times\boldsymbol{U}^* - \nu\Delta^*\boldsymbol{U}^* &= \boldsymbol{f}^*,\\ \nabla^*\cdot\boldsymbol{U}^* &= 0, \end{aligned}\right\} \tag{2.1}$$

where $\Delta^* \equiv (\nabla^*)^2$, all starred quantities are dimensional, and $\boldsymbol{U}^* = (U^*, V^*, W^*)$ is the velocity, ρ^* the density, π^* the pressure, and ν the kinematic viscosity of the fluid. We denote the time variable as, t^* and space variables as (X^*, Y^*, Z^*). For ease of notation, we also introduce $\boldsymbol{X}^* := (X^*, Y^*)$, the horizontal position vector. The function $\boldsymbol{f}^*$ is a forcing term sustaining the mainstream flow (such as an imposed pressure gradient). The domain Ω^* occupied by the fluid is described in the following section.

2.2. *The wavy boundary*

We now investigate the formation of boundary layers next to the wavy boundary. We consider small-scale variations of the boundary, and describe how they can affect the Ekman layer, and the associated Ekman pumping. We will use an idealized model assuming periodic variations of the boundary, this simpler case being already rather interesting from a physical point of view. Non-periodic boundaries will be briefly discussed in § 6.

Let us consider a domain Ω^* of the following form:

$$\Omega^* := \{(\boldsymbol{X}^*, Z^*),\, \Gamma^*(\boldsymbol{X}^*) < Z^* < L^*\}, \tag{2.2}$$

where Γ^* is a function describing the lower boundary, and L^* is a positive constant. The system (2.1) is completed with boundary conditions at the top and bottom of the domain,

$$z\cdot\boldsymbol{U}^* = 0 \quad\text{and}\quad z\cdot\nabla(z\times\boldsymbol{U}^*) = \boldsymbol{0} \qquad \text{at the upper boundary (stress-free),} \tag{2.3a}$$

$$\boldsymbol{U}^* = \boldsymbol{0} \qquad \text{at the lower boundary (no-slip).} \tag{2.3b}$$

We denote the maximal amplitude, X^*–periodicity, and Y^*–periodicity of the wavy boundary as h^*, l_X^*, and l_Y^* respectively. The typical size of the Ekman layer is $L^*E^{1/2} = (\nu/\Omega)^{1/2}$, where E is the Ekman number. It is therefore convenient to introduce α, λ_x and λ_y such that

$$h^* = \alpha L^* E^{1/2}, \quad l_X^* = \lambda_x L^* E^{1/2}, \quad l_Y^* = \lambda_y L^* E^{1/2}. \tag{2.4a}$$

https://doi.org/10.1017/S0022112006001856 Published online by Cambridge University Press

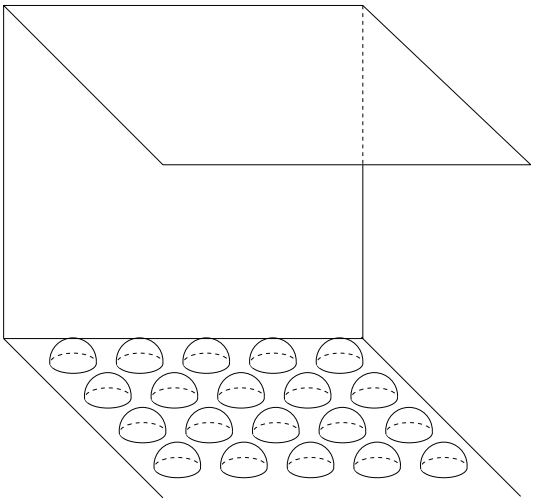


FIGURE 1. Schematic of the fluid flow investigated in a rotating reference frame in a domain Ω with a modulated bottom boundary and flat top boundary.

2.3. *Dimensionless equations*

We now introduce dimensionless quantities

$$\boldsymbol{X} = \boldsymbol{X}^*/L^*, \quad Z = Z^*/L^*, \quad t = t^*U^*/L^*, \tag{2.5a}$$

where U^* is the typical flow velocity. We also define

$$\boldsymbol{U} = (U, V, W) = \boldsymbol{U}^*/U^*, \quad \pi = \pi^*/(\rho^*\Omega U^* L^*), \quad \boldsymbol{f} = \boldsymbol{f}^* L^*/(U^*)^2. \tag{2.5b}$$

The governing equations then become

$$\left.\begin{aligned} \varepsilon\,(\partial_t \boldsymbol{U} + \boldsymbol{U}\cdot\nabla\boldsymbol{U}) + \nabla\pi + 2\boldsymbol{z}\times\boldsymbol{U} - E\,\Delta\boldsymbol{U} = \varepsilon\,\boldsymbol{f}, \\ \nabla\cdot\boldsymbol{U} = 0, \end{aligned}\right\} \tag{2.6}$$

where the Rossby number, $\varepsilon = U^*/(\Omega L^*)$, and Ekman number E have been used. The domain Ω^* becomes

$$\Omega = \{(\boldsymbol{X}, Z)\,, \Gamma(\boldsymbol{X}) < Z < 1\}, \tag{2.7}$$

as shown in figure 1. The wavy boundary is described by the function

$$\Gamma(\boldsymbol{X}) = \frac{\Gamma^*(L^*\boldsymbol{X})}{L^*}. \tag{2.8}$$

2.4. *Boundary layer construction*

We wish to investigate the behaviour of $\boldsymbol{U}$ for small ε and E. Following the classical approach for boundary layers, we distinguish between the mainstream, or interior, flow, and a boundary layer correction.

2.4.1. *Mainstream solution and boundary layer description*

Far from the boundary, we seek an expansion for $\boldsymbol{U}$ of the form

$$\boldsymbol{U} = \boldsymbol{U}^0(t, \boldsymbol{X}, Z) + E^{1/2}\,\boldsymbol{U}^1(t, \boldsymbol{X}, Z) + \cdots. \tag{2.9}$$

When $\varepsilon/E^{1/2} \leqslant O(1)$ the classical geostrophic balance is recovered:

$$2\boldsymbol{z}\times\boldsymbol{U}^0 + \nabla_{\boldsymbol{X},Z}\Pi^0 = 0, \quad \nabla_{\boldsymbol{X},Z}\cdot\boldsymbol{U}^0 = 0, \tag{2.10}$$

https://doi.org/10.1017/S0022112006001856 Published online by Cambridge University Press

so that $\boldsymbol{U}^0$ does not depend on Z, and $\boldsymbol{V} = (U^0, V^0) = \frac{1}{2}\nabla_X{}^{\perp} \Pi^0$, where $\nabla_X{}^{\perp} = (-\partial_Y, \partial_X)$.

Because the traditional Ekman layer develops on a vertical length scale $E^{1/2}$, it is natural to introduce stretched coordinates. We define

$$x = X/E^{1/2}, \quad y = Y/E^{1/2}, \quad z = Z/E^{1/2}. \tag{2.11}$$

(Note that time is not rescaled.) Near the boundary, we consider an expansion of type

$$\boldsymbol{U} = \boldsymbol{u}^0(t, X, Y, x, y, z) + E^{1/2}\,\boldsymbol{u}^1(t, X, Y, x, y, z) + \cdots \tag{2.12}$$

where all $\boldsymbol{u}^i$ are periodic in the x- and y-directions, with periods λ_x and λ_y respectively. At leading order, the following system is derived:

$$\left.\begin{aligned} \frac{\varepsilon}{E^{1/2}}\,\boldsymbol{u}^0 \cdot \nabla_{\boldsymbol{x},z}\,\boldsymbol{u}^0 + 2\boldsymbol{z} \times \boldsymbol{u}^0 + \nabla_{\boldsymbol{x},z}\,\pi^0 - \Delta_{\boldsymbol{x},z}\,\boldsymbol{u}^0 &= 2\boldsymbol{z} \times \boldsymbol{U}^0, \\ \nabla_{\boldsymbol{x},z} \cdot \boldsymbol{u}^0 &= 0, \end{aligned}\right\} \tag{2.13a}$$

where

$$\nabla_{\boldsymbol{x},z} = (\partial_x, \partial_y, \partial_z), \quad \Delta_{\boldsymbol{x},z} = \partial_x^2 + \partial_y^2 + \partial_z^2. \tag{2.13b}$$

These equations hold in the scaled semi-infinite boundary layer domain

$$\omega = \{(\boldsymbol{x}, z), \quad \alpha\,\gamma\,(\boldsymbol{x}) < z\}, \tag{2.14a}$$

where

$$\gamma : \mathbb{R}^2 \to [0, 1], \quad \alpha\,\gamma\,(\boldsymbol{x}) = \Gamma\big(E^{1/2}\boldsymbol{x}\big)/E^{1/2}. \tag{2.14b}$$

The system is completed with the boundary conditions

$$\boldsymbol{u}^0|_{\partial\omega} = 0, \quad \lim_{z \to +\infty} \boldsymbol{u}^0(t, X, Y, x, y, z) = \boldsymbol{U}^0(t, X, Y). \tag{2.15}$$

Let us make a few comments on this boundary layer system. First, if we integrate the divergence-free condition

$$\nabla_{\boldsymbol{x},z} \cdot \boldsymbol{u}^0 = \partial_x u^0 + \partial_y v^0 + \partial_z w^0 = 0, \tag{2.16}$$

over the whole domain ω, integration by parts yields

$$0 = \int_{\partial\omega} \boldsymbol{n} \cdot \boldsymbol{u}^0 + \lim_{z \to +\infty} \int_{x,y} w^0(t, X, Y, x, y, z)\,\mathrm{d}x\,\mathrm{d}y = \lim_{z \to +\infty} \int_{x,y} w^0(t, X, Y, x, y, z)\,\mathrm{d}x\,\mathrm{d}y, \tag{2.17a}$$

where

$$\int_{x,y} = \frac{1}{\lambda_x\,\lambda_y} \int_0^{\lambda_x} \int_0^{\lambda_y}. \tag{2.17b}$$

Equation (2.15) then implies that $\boldsymbol{U}^0 \cdot \boldsymbol{z} = 0$, just as in the case of a flat boundary. The interior flow $\boldsymbol{U}^0$ must therefore be horizontal:

$$\boldsymbol{U}^0 = (\boldsymbol{V}, 0) = \tfrac{1}{2}(-\partial_Y \Pi, \partial_X \Pi, 0), \tag{2.18}$$

and the mainstream vertical flow vanishes at leading order.

https://doi.org/10.1017/S0022112006001856 Published online by Cambridge University Press

Another interesting similarity with the case of a flat boundary is that t, X, Y act as simple parameters. More precisely, if one 'freezes' (t, X, Y) and denotes for short

$$\boldsymbol{V} = \boldsymbol{V}(t, X, Y), \quad \boldsymbol{u}(x, y, z) = \boldsymbol{u}^0(t, X, Y, x, y, z), \quad p(x, y, z) = \pi^0(t, X, Y, x, y, z), \tag{2.19}$$

one can write system (2.13*a*), (2.15) as

$$\left.\begin{aligned} \frac{\varepsilon}{E^{1/2}}\boldsymbol{u}\cdot\nabla_{\boldsymbol{x},z}\,\boldsymbol{u} + 2\boldsymbol{z}\times\boldsymbol{u} + \nabla_{\boldsymbol{x},z}\,p - \Delta_{\boldsymbol{x},z}\,\boldsymbol{u} &= 2\boldsymbol{z}\times(\boldsymbol{V},0),\\ \nabla_{\boldsymbol{x},z}\cdot\boldsymbol{u} &= 0, \end{aligned}\right\} \tag{2.20a}$$

$$\boldsymbol{u}|_{\partial\omega} = 0, \quad \lim_{z\to+\infty}\boldsymbol{u}(x, y, z) = (\boldsymbol{V}, 0), \tag{2.20b}$$

which yields a boundary value problem with (x, y, z) coordinates, set on the domain ω (with boundary $\partial\omega$), with parameter $\boldsymbol{V}$.

In the classical configuration, with flat boundaries, no dependence on x, y is implied, and therefore $\boldsymbol{u} = \boldsymbol{u}(z)$. System (2.20*a*) simplifies to a system of linear ordinary differential equations, leading to the Ekman spiral. In the case of wavy boundaries, however, (2.20*a*) is a genuine system of partial differential equations. It is of Stokes type for $\varepsilon/E^{1/2} \ll 1$, and of Navier–Stokes type for $\varepsilon/E^{1/2} = O(1)$. This considerably affects the dynamical properties of the fluid inside and outside the boundary layer, as will be shown in what follows. This also makes the mathematical analysis of (2.20) more difficult, as no analytical expression is available. Such an analysis has been partly carried out by one of the authors (Gérard-Varet 2003). In particular, it has been shown that, for $\boldsymbol{V}$ such that

$$Re = \frac{\varepsilon|\boldsymbol{V}|}{E^{1/2}} \quad \text{sufficiently small}, \tag{2.21}$$

system (2.20) has a unique smooth solution $\boldsymbol{u}$. Moreover, this solution converges exponentially to $\boldsymbol{V}$ as z goes to $+\infty$ (see Gérard-Varet 2003 for a precise mathematical statement). Note that $Re = (U^*|\boldsymbol{V}|)\,L^*\,E^{1/2}/\nu$ is a Reynolds number based on the Ekman layer size, so that assumption (2.21) is a classical condition of hydrodynamic stability. Under this assumption, we can introduce (following Dormy, Roberts & Soward 2005) the volume flux deficit in the boundary layer:

$$\boldsymbol{Q}_\parallel = \int_{\alpha\gamma(\boldsymbol{x})}^{\infty}(\boldsymbol{u}_\parallel - \boldsymbol{V})\,\mathrm{d}z = \int_{\alpha\gamma(\boldsymbol{x})}^{\infty}((u, v) - \boldsymbol{V})\,\mathrm{d}z, \tag{2.22}$$

which depends on both $\boldsymbol{x}$ and $\boldsymbol{V}$. The global flux deficit is then given by

$$\boldsymbol{\mathcal{Q}}_\parallel(\boldsymbol{V}) = \int_{\boldsymbol{x}}\boldsymbol{Q}_\parallel\,\mathrm{d}\boldsymbol{x}, \tag{2.23}$$

and depends only on $\boldsymbol{V}$. As $\boldsymbol{V}$ is a function of (t, X, Y), then $\boldsymbol{\mathcal{Q}}_\parallel(\boldsymbol{V})$ is a two-dimensional vector field depending on t, X, Y.

2.5. *The Ekman pumping*

Our main concern in this paper is the qualitative behaviour of the boundary layer, and the consequence of wavy boundaries for Ekman pumping. Although the roughness makes the vertical component of the leading-order velocity non-zero in the layer, this component vanishes at infinity ($\lim_{z\to+\infty} w^0 = 0$). The Ekman pumping is $O(E^{1/2})$, as in the case of flat boundaries. More precisely, writing $\boldsymbol{u} = \boldsymbol{u}^0 + E^{1/2}\boldsymbol{u}^1 + o(E^{1/2})$, we

https://doi.org/10.1017/S0022112006001856 Published online by Cambridge University Press

obtain

$$\nabla_{x,z} \cdot \boldsymbol{u}^1 = -\partial_X u^0 - \partial_Y v^0. \tag{2.24}$$

An integration by parts over the domain ω leads to

$$\lim_{z \to +\infty} \int_{x,y} w^1 = -\partial_X \int_\omega (u^0 - U^0) - \partial_Y \int_\omega (v^0 - V^0). \tag{2.25}$$

Provided that $\varepsilon |\boldsymbol{V}(t, X, Y)| / E^{1/2}$ remains small enough, the pumping is expressed as

$$\lim_{z \to +\infty} \int_{x,y} w^1(t, X, Y, x, y, z)\, \mathrm{d}x\, \mathrm{d}y = -\nabla_{\boldsymbol{X}} \cdot \boldsymbol{\mathcal{Q}}_\parallel(\boldsymbol{V}), \tag{2.26a}$$

where

$$\nabla_{\boldsymbol{X}} \cdot \boldsymbol{g} = \partial_X g_1 + \partial_Y g_2 = \boldsymbol{n} \cdot \nabla \times (\boldsymbol{n} \times \boldsymbol{g}). \tag{2.26b}$$

In the case of flat boundaries, $\boldsymbol{\mathcal{Q}}_\parallel$ simplifies to

$$\boldsymbol{\mathcal{Q}}_\parallel(\boldsymbol{V}) = \tfrac{1}{2}(\boldsymbol{V}^\perp - \boldsymbol{V}) \tag{2.27}$$

(resulting from the Ekman spiral). One thus recovers the classical Ekman pumping

$$w = \tfrac{1}{2} E^{1/2} \nabla_{\boldsymbol{X}} \cdot (\boldsymbol{V} - \boldsymbol{V}^\perp) = \tfrac{1}{2} E^{1/2} \nabla_{\boldsymbol{X}} \times \boldsymbol{V}. \tag{2.28}$$

We consider rough boundaries that are free of large-scale topography $H(X, Y)$, so that the horizontal roughness depends only on (x, y). As a result, no term of the form $\boldsymbol{V} \cdot \nabla H$ is present in (2.26*a*).

When the boundary is wavy, the resulting expression in (2.26*a*) is not explicit. The steady profile thus depends nonlinearly on $\boldsymbol{V}$ when $\varepsilon / E^{1/2} = O(1)$. One can, however, retrieve a simpler expression by assuming both small-amplitude flow ($\varepsilon / E^{1/2} < O(1)$ in (2.20*a*)) and isotropic roughness. Linearization on the basis of a small-amplitude flow provides

$$\boldsymbol{\mathcal{Q}}_\parallel(\boldsymbol{V}) = \boldsymbol{\mathcal{Q}}_\parallel \boldsymbol{V}, \tag{2.29}$$

where $\boldsymbol{\mathcal{Q}}_\parallel$ is a 2×2 matrix. In the case of isotropic roughness, the matrix $\boldsymbol{\mathcal{Q}}_\parallel$ commutes to rotations which implies

$$\boldsymbol{\mathcal{Q}}_\parallel = \begin{pmatrix} a & b \\ -b & a \end{pmatrix}, \text{ with } (a, b) \in \mathbb{R}^2, \tag{2.30}$$

and the Ekman pumping is thus very similar to the usual expression (2.28),

$$w = E^{1/2} b \nabla_{\boldsymbol{X}} \times \boldsymbol{V}. \tag{2.31}$$

2.5.1. *The quasi-geostrophic equations*

All quantities described above depend only on the interior flow $\boldsymbol{U}^0 = (\boldsymbol{V}, 0)$. The equations satisfied by $\boldsymbol{V} = \frac{1}{2} \nabla_{\boldsymbol{X}}^\perp \Pi$ remain to be established. Writing

$$\boldsymbol{u} = \boldsymbol{U}^0 + E^{1/2} \boldsymbol{U}^1 + o\big(E^{1/2}\big), \tag{2.32}$$

one obtains

$$\partial_t \boldsymbol{U}^0 + \boldsymbol{U}^0 \cdot \nabla_{\boldsymbol{X},Z} \boldsymbol{U}^0 + \frac{E^{1/2}}{\varepsilon} (2\boldsymbol{z} \times \boldsymbol{U}^1 + \nabla_{\boldsymbol{X},Z} \Pi^1) = (f_1, f_2, 0). \tag{2.33}$$

https://doi.org/10.1017/S0022112006001856 Published online by Cambridge University Press

Considering the vertical component of the curl of this equation yields

$$\partial_t \Delta_X \Pi + \boldsymbol{V}\cdot\nabla_X \Delta_X \Pi - 4\frac{E^{1/2}}{\varepsilon}\partial_Z W^1 = 2\partial_X f_2 - 2\partial_Y f_1. \tag{2.34a}$$

Integration with respect to Z from $Z=\sup\Gamma$ to $Z=1$, and with respect to $\boldsymbol{x}$ over a period leads to

$$\partial_t \Delta_X \Pi + \boldsymbol{V}\cdot\nabla_X \Delta_X \Pi + 4\frac{E^{1/2}}{\varepsilon}\lim_{z\to+\infty}\int_{\boldsymbol{x}} w^1 = 2\int_0^1 (\partial_X f_2 - \partial_Y f_1)\,\mathrm{d}z. \tag{2.34b}$$

Using (2.26*a*), we deduce

$$\left.\begin{aligned} \partial_t \Delta_X \Pi + \boldsymbol{V}\cdot\nabla_X \Delta_X \Pi - 4\frac{E^{1/2}}{\varepsilon}\nabla_X\cdot\boldsymbol{\mathcal{Q}}_{\parallel}(\boldsymbol{V}) = 2\int_0^1 (\partial_X f_2 - \partial_Y f_1)\,,\\ \boldsymbol{V} = \tfrac{1}{2}\nabla_X^{\perp}\Pi. \end{aligned}\right\} \tag{2.34c}$$

These are the classical quasi-geostrophic equations of relative vorticity, in which Ekman pumping is modified by the roughness of the boundaries. It involves the function $\boldsymbol{\mathcal{Q}}_{\parallel}$, defined in (2.23), related to the boundary layer system (2.20).

2.5.2. *Relation between dissipation and friction*

We should stress here the relationship among Ekman pumping, energy dissipation in the quasi-geostrophic flow, and friction in the boundary layer.

On the one hand, multiplying equation (2.34*c*) by Π, and integrating with respect to $\boldsymbol{X}$ yields (we assume that $f=0$ for simplicity)

$$\partial_t\left(\int_{X,Y}|\boldsymbol{V}(t,\cdot)|^2\right) + 2\frac{E^{1/2}}{\varepsilon}\int_{X,Y}\boldsymbol{\mathcal{Q}}_{\parallel}(\boldsymbol{V}(t,\cdot))\cdot\boldsymbol{V}^{\perp}(t,\cdot) = 0, \quad \boldsymbol{V}^{\perp} = (-V, U). \tag{2.35}$$

On the other hand, one can show that, for all $\boldsymbol{V}$,

$$\int_{\omega}|\nabla\boldsymbol{u}|^2 = 2\,\boldsymbol{\mathcal{Q}}_{\parallel}(\boldsymbol{V})\cdot\boldsymbol{V}^{\perp}, \tag{2.36}$$

where $\boldsymbol{u}$ is the solution of (2.20), and $|\nabla\boldsymbol{u}|$ is the quadratic norm of the gradient matrix. We refer to Gérard-Varet (2003) for a proof of this equality. Reverting to the original variables, this implies

$$\int_{X,Y}\int_{\omega}|\nabla_{\boldsymbol{x},z}\boldsymbol{u}^0(t,\cdot)|^2 = 2\int_{X,Y}\boldsymbol{\mathcal{Q}}_{\parallel}(\boldsymbol{V}(t,\cdot))\cdot\boldsymbol{V}^{\perp}(t,\cdot), \tag{2.37a}$$

and

$$\partial_t\left(\int_{X,Y}|\boldsymbol{V}(t,\cdot)|^2\right) = -\frac{E^{1/2}}{\varepsilon}\int_{X,Y}\int_{\omega}|\nabla_{\boldsymbol{x},z}\,\boldsymbol{u}^0(t,\cdot)|^2. \tag{2.37b}$$

One thus verifies that, at leading order, the kinetic energy dissipation in the geostrophic flow is due to friction in the boundary layer. Moreover, it is linked to the Ekman pumping through the function $\boldsymbol{\mathcal{Q}}_{\parallel}$. The crucial quantity is

$$\mathscr{E}(\boldsymbol{V}) = 2\,(\boldsymbol{\mathcal{Q}}_{\parallel}(\boldsymbol{V})\cdot\boldsymbol{V}^{\perp})/|\boldsymbol{V}|^2. \tag{2.38}$$

Note that in the case of a flat horizontal boundary, this simplifies to

$$\mathscr{E}(\boldsymbol{V}) = ((\boldsymbol{V}^{\perp}-\boldsymbol{V})\cdot\boldsymbol{V}^{\perp})/|\boldsymbol{V}|^2 = 1. \tag{2.39}$$

https://doi.org/10.1017/S0022112006001856 Published online by Cambridge University Press

$\mathscr{E}(\boldsymbol{V})$ which depends on X, Y through $\boldsymbol{V}$ corresponds to a local estimate of the energy dissipation, or equivalently to a local estimate of the friction in the layer. Note that it can also provide some partial information on the Ekman pumping. In the case of a planar boundary, as in the case of an isotropic roughness and small-amplitude flow, it is because the flux deficit $\boldsymbol{\mathcal{Q}}_{\parallel}$ does not lie in the direction of the mainstream flow $\boldsymbol{V}$ that the pumping $\nabla_X \cdot \boldsymbol{\mathcal{Q}}_{\parallel}$ does not vanish. More precisely, following the linear reasoning of (2.31), one easily verifies that the resulting Ekman pumping is $\nabla_X \cdot \boldsymbol{\mathcal{Q}}_{\parallel} = \frac{1}{2}\mathscr{E}\,\nabla \times \boldsymbol{V}$.

If the mainstream flow $\boldsymbol{V}$ is uniform, there is no net pumping associated with the boundary layer. However, the flux deficit $\boldsymbol{\mathcal{Q}}_{\parallel}$ and the energy dissipation $\mathscr{E}$ remain well-defined quantities. $\mathscr{E}(\boldsymbol{V})$ is then a relevant quantity, not only as an estimate of dissipation, but also as an estimate of the Ekman pumping that will result from a variation of $\boldsymbol{V}$ with X and Y. If the roughness is anisotropic, however, the component of $\boldsymbol{\mathcal{Q}}_{\parallel}$ along the direction of $\boldsymbol{V}$ will also contribute to the Ekman pumping (but obviously not to the energy dissipation).

We shall now focus our attention on the analysis of $\mathscr{E}$ for various types of roughness and constant velocities at infinity $\boldsymbol{V}$. Thus, with a proper choice of U^*, one can set $|\boldsymbol{V}| = 1$. Special attention will be paid to whether $\mathscr{E} < 1$ or $\mathscr{E} > 1$, i.e. whether dissipation is decreasing or increasing with respect to the case of a flat horizontal boundary. We will limit consideration to small $Re = \varepsilon/E^{1/2}$, for which linearization of the equations is possible. In this regime, the boundary layer equations become

$$\left.\begin{aligned} 2\boldsymbol{z} \times \boldsymbol{u} + \nabla p - \Delta\, \boldsymbol{u} &= 2\boldsymbol{z} \times (\boldsymbol{V}, 0), \\ \nabla \cdot \boldsymbol{u} &= 0, \end{aligned}\right\} \tag{2.40a}$$

$$\boldsymbol{u}|_{\partial\omega} = 0, \quad \lim_{z \to +\infty} \boldsymbol{u}(\boldsymbol{x}, z) = (\boldsymbol{V}, 0), \tag{2.40b}$$

where the notation $\nabla = \nabla_{\boldsymbol{x},z}$ and $\Delta = \Delta_{\boldsymbol{x},z}$ will be used throughout.

The system (2.40) being linear, $\boldsymbol{\mathcal{Q}}_{\parallel}(\boldsymbol{V}) = \boldsymbol{\mathcal{Q}}_{\parallel}\boldsymbol{V}$, and since $|\boldsymbol{V}| = 1$, the vector $\boldsymbol{V}$ takes the form

$$\boldsymbol{V} = (\cos\varphi, \sin\varphi), \quad \varphi \geqslant 0. \tag{2.41}$$

We will study the dependence of $\mathscr{E}$ on the angle φ of the mainstream flow, on the amplitude α and on the wavelengths λ_x, λ_y of the roughness. The effect of nonlinearities on $\boldsymbol{\mathcal{Q}}_{\parallel}$ is the subject of a forthcoming paper.

3. Amplitude analysis

In this section, we study the case of small-amplitude wavy boundaries of the form

$$\partial\omega = \{(\boldsymbol{x}, z), \quad z = \alpha\gamma(\boldsymbol{x})\}, \tag{3.1}$$

with $\alpha \ll 1$ and γ smooth. In this framework, one can compute the solution $\boldsymbol{u}$ of (2.40) using an asymptotic expansion.

Let us first make the following change of variable:

$$z \mapsto z - \alpha\gamma(\boldsymbol{x}), \tag{3.2}$$

so that ω becomes the half-plane $\omega_+ = \{z > 0\}$. The boundary layer system is expressed in these new variables as

$$\left.\begin{aligned} 2\boldsymbol{z} \times \boldsymbol{u}_\alpha + \nabla_\alpha p_\alpha - \Delta_\alpha\, \boldsymbol{u}_\alpha &= 2\boldsymbol{z} \times (\boldsymbol{V}, 0), \\ \nabla_\alpha \cdot \boldsymbol{u}_\alpha &= 0, \end{aligned}\right\} \tag{3.3a}$$

$$\boldsymbol{u}_\alpha|_{z=0} = 0, \quad \lim_{z \to +\infty} \boldsymbol{u}_\alpha(\boldsymbol{x}, z) = (\boldsymbol{V}, 0), \tag{3.3b}$$

https://doi.org/10.1017/S0022112006001856 Published online by Cambridge University Press

where

$$\boldsymbol{u}(\boldsymbol{x}, z) = \boldsymbol{u}_\alpha(\boldsymbol{x}, z - \alpha\gamma(\boldsymbol{x})), \quad \nabla_\alpha = \nabla + \alpha(-\gamma_x\partial_z, -\gamma_y\partial_z, 0), \quad \Delta_\alpha = \nabla_\alpha \cdot \nabla_\alpha. \tag{3.3c}$$

3.1. *Asymptotic expansion*

In view of (3.3), it is then natural to seek an expansion of the form

$$\boldsymbol{u}_\alpha = \boldsymbol{u}_0 + \alpha\,\boldsymbol{u}_1 + \cdots. \tag{3.4}$$

We first identify $O(1)$ terms in (3.3), yielding

$$\left.\begin{aligned} 2\boldsymbol{z} \times \boldsymbol{u}_0 + \nabla p_0 - \Delta\,\boldsymbol{u}_0 = 2(\boldsymbol{V}^\perp, 0), \\ \nabla \cdot \boldsymbol{u}_0 = 0, \end{aligned}\right\} \tag{3.5a}$$

$$\boldsymbol{u}_0|_{z=0} = 0, \quad \lim_{z\to+\infty} \boldsymbol{u}_0(\boldsymbol{x}, z) = (\boldsymbol{V}, 0). \tag{3.5b}$$

We find that $\boldsymbol{u}_0 = \boldsymbol{u}_{\boldsymbol{V}}(z)$ is the classical Ekman spiral

$$w_{\boldsymbol{V}} = 0, \quad u_{\boldsymbol{V}} + \mathrm{i}v_{\boldsymbol{V}} = \exp(\mathrm{i}\varphi)[1 - \exp((-1 - \mathrm{i})z)]. \tag{3.6}$$

We then identify $O(\alpha)$ terms to obtain

$$\left.\begin{aligned} 2\boldsymbol{z} \times \boldsymbol{u}_1 + \nabla p_1 - \Delta\,\boldsymbol{u}_1 = -(\gamma_{xx} + \gamma_{yy})\,\partial_z \boldsymbol{u}_0, \\ \nabla \cdot \boldsymbol{u}_1 = \gamma_x \partial_z u_0 + \gamma_y \partial_z v_0. \end{aligned}\right\} \tag{3.7}$$

Similarly, the $O(\alpha^i)$ terms provide equations for $\boldsymbol{u}_i$, $i \geqslant 2$. Note that these equations are all of Ekman type, with the Coriolis force and source terms due to the lower $\boldsymbol{u}_k$, $k < i$. They are completed with the homogeneous boundary conditions

$$\boldsymbol{u}_i|_{z=0} = 0, \quad \boldsymbol{u}_i|_{z=+\infty} = 0. \tag{3.8}$$

These equations can be solved analytically using an Orr–Sommerfeld formulation. By introducing

$$\varphi_i = \partial_x v_i - \partial_y u_i, \tag{3.9}$$

the pressure term can be dropped and, after differentiation, one obtains

$$-2\partial_z w_i - \Delta\varphi_i = f_i, \quad 2\partial_z \varphi_i - \Delta^2 w_i = g_i, \tag{3.10a}$$

where φ_i, w_i and $\partial_z w_i$ are prescribed at the boundaries:

$$\left.\begin{aligned} &\varphi_i = w_i = \partial_z w_i = 0 && \text{for} \quad z \to \infty, \\ &\varphi_i = w_i = 0, \quad \partial_z w_i = \gamma_x \partial_z u_{i-1} + \gamma_y \partial_z v_{i-1} && \text{for} \quad z = 0. \end{aligned}\right\} \tag{3.10b}$$

On performing a Fourier transform on the tangential variables x, y, (3.10a) reduces to a differential system in variable z. In this way, one can compute the $\boldsymbol{u}_i$ recursively. Restoring the original variables,

$$\boldsymbol{u}(\boldsymbol{x}, z) = \boldsymbol{u}_0(\boldsymbol{x}, z - \alpha\gamma(\boldsymbol{x})) + \alpha\,\boldsymbol{u}_1(\boldsymbol{x}, z - \alpha\gamma(\boldsymbol{x})) + \cdots \tag{3.11}$$

$$= \tilde{\boldsymbol{u}}_0(\boldsymbol{x}, z) + \alpha\,\tilde{\boldsymbol{u}}_1(\boldsymbol{x}, z) + \cdots. \tag{3.12}$$

Note that the first term of the expansion $\tilde{\boldsymbol{u}}_0 = \boldsymbol{u}_0$ still corresponds to the Ekman spiral. The expansion is justified provided

$$\alpha \ll 1, \quad \lambda_x, \lambda_y = O(1) \text{ or } \lambda_x, \lambda_y \gg 1. \tag{3.13}$$

When λ_x, λ_y go to zero, equations (3.7) and those following degenerate. The analysis therefore loses its validity in this limit.

https://doi.org/10.1017/S0022112006001856 Published online by Cambridge University Press

3.2. *Dissipation*

From the asymptotic expansion, one can recover some interesting features of

$$\mathscr{E}(\boldsymbol{V}) = 2\int_{\omega} ((u, v) - \boldsymbol{V}) \cdot \boldsymbol{V}^{\perp}, \tag{3.14}$$

for α sufficiently small. One can write

$$\begin{aligned}\mathscr{E}(\boldsymbol{V}) &= 2\int_{\omega_+} ((u_\alpha, v_\alpha) - \boldsymbol{V})^{\perp} \cdot \boldsymbol{V} \\ &\approx 2\int_{\omega_+} ((u_0, v_0) - \boldsymbol{V})^{\perp} \cdot \boldsymbol{V} + 2\alpha \int_{\omega_+} (u_1, v_1)^{\perp} \cdot \boldsymbol{V} + 2\alpha^2 \int_{\omega_+} (u_2, v_2)^{\perp} \cdot \boldsymbol{V}. \end{aligned} \tag{3.15}$$

The first term in the right-hand side is unity, as it stems from the classical Ekman pumping. Integration of equations (3.7) then yields

$$2\int_{\boldsymbol{x}} (u_1, v_1)^{\perp} - \partial_z^2 \int_{\boldsymbol{x}} (u_1, v_1) = 0, \tag{3.16a}$$

$$\partial_z \int_{\boldsymbol{x}} w_1 = 0, \quad \boldsymbol{u}_1|_{z=0,+\infty} = 0. \tag{3.16b}$$

Therefore $\int_{\boldsymbol{x}} \boldsymbol{u}_1 = 0$, and $\int_{\omega_+} (u_1, v_1) \cdot \boldsymbol{V}^{\perp} = 0$. Finally, one obtains

$$\mathscr{E}(\boldsymbol{V}) = 1 + \alpha^2 \mathscr{C}(\varphi, \gamma), \tag{3.17}$$

where $\mathscr{C}(\varphi, \gamma) = 2\int_{\omega_+} (u_2, v_2) \cdot \boldsymbol{V}^{\perp}$ depends on the vector $\boldsymbol{V} = (\cos(\varphi), \sin(\varphi))$ and the boundary γ. Hence, if the roughness is $O(\alpha)$ with α small enough, the friction changes at $O(\alpha^2)$. More precisely, the analytic computations provide

$$\mathscr{C}(\varphi, \gamma) = \sum_{\boldsymbol{k}} |\hat{\gamma}(\boldsymbol{k})|^2 C\left(k, \left|\frac{\boldsymbol{k}}{k} \cdot \boldsymbol{V}\right|\right), \tag{3.18}$$

with the Fourier coefficients of γ,

$$\hat{\gamma}(\boldsymbol{k}) = \int_{\boldsymbol{x}} \mathrm{e}^{-\mathrm{i}\boldsymbol{k}\cdot\boldsymbol{x}} \gamma(\boldsymbol{x})\, \mathrm{d}\boldsymbol{x}, \quad \boldsymbol{k} = (k_x, k_y),\ k_x \in (2\pi/\lambda_x)\mathbb{Z},\ k_y \in (2\pi/\lambda_y)\mathbb{Z}. \tag{3.19}$$

The coefficient $C(k, \theta)$ is a function of the wave vector modulus $k = |\boldsymbol{k}| = \sqrt{k_x^2 + k_y^2}$ and the variable $\theta = |\boldsymbol{k}/|\boldsymbol{k}| \cdot \boldsymbol{V}|$, which measures the inclination of the wave vector with respect to $\boldsymbol{V}$. Figure 2 presents plots of the function

$$f : (k, \theta) \mapsto \frac{C(k, \theta)}{1 + k^4}. \tag{3.20}$$

Note that f goes to zero in the limit of small and large k, and takes both positive and negative values. One can draw two conclusions from this:

Remark 1. For small enough α, the minimal and maximal dissipations are reached with one-dimensional boundaries $\gamma = \gamma(x)$.

Let us clarify this statement. By minimal and maximal, we mean minimal and maximal among all angles φ and all smooth boundaries γ with $O(1)$ amplitude. To be more precise, we must have a normalization condition on boundaries γ, for the loose statement $\gamma = O(1)$ to be quantified. Although any normalization ensuring the

https://doi.org/10.1017/S0022112006001856 Published online by Cambridge University Press

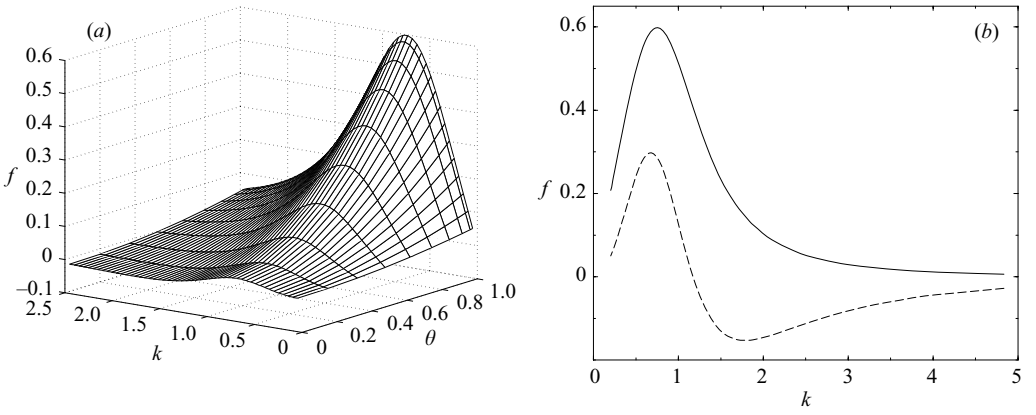


FIGURE 2. The correction term $f(k,\theta)$: (*a*) the whole surface f; (*b*) $k \mapsto f(k,\theta)$ for $\theta = 1$ (solid line) and $\theta = 0$, scaled by a factor 10 for clarity (dashed line).

regularity of γ will lead to the above conclusion, a convenient choice is

$$\sum_{\boldsymbol{k}} (1 + |\boldsymbol{k}|^4)\, |\hat{\gamma}(\boldsymbol{k})|^2 = 1. \tag{3.21}$$

This can be verified by computing the following quantities:

$$\max_{\substack{\varphi\in[0,2\pi],\\ \gamma\in\mathscr{X}}} \mathscr{C}(\varphi,\gamma), \qquad \min_{\substack{\varphi\in[0,2\pi],\\ \gamma\in\mathscr{X}}} \mathscr{C}(\varphi,\gamma), \tag{3.22}$$

where $\mathscr{X} = \{\gamma \text{ smooth}, \gamma \text{ satisfies (3.21)}\}$. The maximal and minimal dissipations are then deduced from (3.17). One can write

$$\mathscr{C}(\varphi,\gamma) = \sum_{\boldsymbol{k}} (1 + |\boldsymbol{k}|^4)\, |\hat{\gamma}(\boldsymbol{k})|^2 f\left(|\boldsymbol{k}|, \left|\frac{\boldsymbol{k}}{|\boldsymbol{k}|}\cdot\boldsymbol{V}\right|\right), \tag{3.23a}$$

so that

$$\max_{\substack{\varphi\in[0,2\pi],\\ \gamma\in\mathscr{X}}} \mathscr{C}(\varphi,\gamma) \leqslant \max_{\substack{\theta\in[0,1],\\ k\geqslant 0}} f(k,\theta), \tag{3.23b}$$

$$\min_{\substack{\varphi\in[0,2\pi],\\ \gamma\in\mathscr{X}}} \mathscr{C}(\varphi,\gamma) \geqslant \min_{\substack{\theta\in[0,1],\\ k\geqslant 0}} f(k,\theta). \tag{3.23c}$$

Denoting as (k_M,θ_M), resp. (k_m,θ_m), the points at which f is extremal, $f(k_M,\theta_M) = \max f(k,\theta)$, resp. $f(k_m,\theta_m) = \min f(k,\theta)$, from figure 2 one can estimate $k_M \approx 0.7$, $\theta_M = 1$, $k_m \approx 2$, $\theta_m = 0$. We then introduce

$$\boldsymbol{k}_M = (k_M, 0), \quad \boldsymbol{k}_m = (k_m, 0), \quad \varphi_M = \arccos(\theta_M) = 0, \quad \varphi_m = \arccos(\theta_m) = \pi/2, \tag{3.24}$$

and the corresponding boundaries

$$\gamma_M = \frac{\mathrm{e}^{\mathrm{i}\boldsymbol{k}_M\cdot\boldsymbol{x}} + \mathrm{e}^{-\mathrm{i}\boldsymbol{k}_M\cdot\boldsymbol{x}}}{2\left(1+k_M^4\right)} = \frac{\cos(k_M x)}{1+k_M^4}, \quad \gamma_m = \frac{\cos(k_m x)}{1+k_m^4}; \tag{3.25}$$

https://doi.org/10.1017/S0022112006001856 Published online by Cambridge University Press

γ_M and γ_m are one-dimensional boundaries. Moreover, using (3.18), we have

$$\mathscr{C}(\varphi_M, \gamma_M) = f(k_M, \theta_M) = \max f(k, \theta), \tag{3.26a}$$

$$\mathscr{C}(\varphi_m, \gamma_m) = f(k_m, \theta_m) = \min f(k, \theta). \tag{3.26b}$$

We deduce that

$$\mathscr{C}(\varphi_M, \gamma_M) = \max \mathscr{C}(\varphi, \gamma), \quad \mathscr{C}(\varphi_m, \gamma_m) = \min \mathscr{C}(\varphi, \gamma), \tag{3.27a}$$

which proves the above remark.

Remark 2. The dissipation may be strictly less than unity.

This stems from f taking negative values. More precisely, from the curve of figure 2(*b*) one notes that $f(k_m, 0) < 0$. Let us introduce as previously

$$\varphi_m = \frac{\pi}{2}, \quad \gamma_m = \frac{\cos(k_m x)}{1 + k_m^4}. \tag{3.28}$$

This implies $\mathscr{C}(\frac{1}{2}\pi, \gamma_m) = f(k_m, 0) < 0$, and the corresponding dissipation is strictly less than unity.

In physical terms, this means that the roughness may decrease the dissipation. The physical interpretation of this phenomenon will be given in § 5, when dealing with general amplitudes and numerical results. A comparison of the small-amplitude analysis and the numerics is also postponed to § 5.

Stressing again that the above small-amplitude analysis does not hold when $\lambda_x, \lambda_y \to 0$, we will perform a small-wavelength analysis in the next section.

4. Wavelength analysis

Throughout the rest of the paper, we limit our investigation to boundaries independent of one coordinate (say y):

$$\partial\omega = \{(x, z), \quad z = \alpha\gamma(x)\}, \tag{4.1}$$

so that φ as defined in (2.41) measures the angle between the boundary profile direction and the mainstream flow. Focusing on one-dimensional boundaries is a natural approach in the light of § 3: at low amplitude α, all interesting features are captured with such configurations.

We wish to analyse the behaviour of the boundary layer when the roughness wavelength becomes very small ($\lambda \ll 1$). For clarity, we set $\alpha = 1$. To emphasize the role of the small parameter λ, let us introduce the fast variable $\tilde{x} = x/\lambda$. The system (2.40) becomes

$$\left.\begin{aligned} &2\boldsymbol{z} \times \boldsymbol{u}_\lambda + \left(\frac{1}{\lambda}\partial_{\tilde{x}} p_\lambda, 0, \partial_z p_\lambda\right) - \left(\frac{1}{\lambda^2}\partial_{\tilde{x}}^2 + \partial_z^2\right)\boldsymbol{u}_\lambda = 2\boldsymbol{z} \times (\boldsymbol{V}, 0), \\ &\frac{1}{\lambda}\partial_{\tilde{x}} u_\lambda + \partial_z w_\lambda = 0, \\ &\boldsymbol{u}_\lambda = 0 \text{ for } z = \tilde{\gamma}(\tilde{x}), \quad \lim_{z \to +\infty} \boldsymbol{u}_\lambda(\tilde{x}, z) = (\boldsymbol{V}, 0), \end{aligned}\right\} \tag{4.2}$$

where $\tilde{\gamma}(\tilde{x}) = \gamma(\lambda\tilde{x})$ has wavelength unity.

As usual, one can expect an asymptotic behaviour of the type:

$$\boldsymbol{u}_\lambda(\tilde{x}, z) = \boldsymbol{u}_0(\tilde{x}, z) + \text{higher order terms in } \lambda. \tag{4.3}$$

https://doi.org/10.1017/S0022112006001856 Published online by Cambridge University Press

The leading equations are

$$-\partial_{\tilde{x}}^2(v_0, w_0) = 0, \quad \partial_{\tilde{x}} u_0 = 0. \tag{4.4}$$

They yield different behaviours for $\boldsymbol{u}_0$, depending on whether $z < \max \tilde{\gamma}$ or $z > \max \tilde{\gamma}$. For all $z < \max \tilde{\gamma}$, i.e. inside the humps, equations (4.4) are completed with Dirichlet boundary conditions

$$\boldsymbol{u}_0(\tilde{x}, z) = 0, \text{ for } \tilde{x} \text{ such that } \tilde{\gamma}(\tilde{x}) = z. \tag{4.5}$$

It follows that

$$\boldsymbol{u}_0 = 0 \text{ for all } z < \max \tilde{\gamma}. \tag{4.6}$$

For all $z > \max \tilde{\gamma}$, i.e. outside the humps, only periodic boundary conditions hold. Equations (4.4) provide

$$\boldsymbol{u}_0 = \overline{\boldsymbol{u}}_0(z) \text{ for all } z > \max \tilde{\gamma}. \tag{4.7}$$

To determine the equation satisfied by $\overline{\boldsymbol{u}}_0$, one can average equations (4.2), and retain only $O(1)$ terms:

$$2(\overline{u}_0, \overline{v}_0)^\perp - \partial_z^2(\overline{u}_0, \overline{v}_0) = 2\boldsymbol{V}^\perp, \tag{4.8a}$$

$$\partial_z \overline{w}_0 = 0, \quad \overline{\boldsymbol{u}}_0 \xrightarrow[z \to +\infty]{} (\boldsymbol{V}, 0). \tag{4.8b}$$

Moreover, by continuity, $\overline{\boldsymbol{u}}_0 = 0$ at $z = \max \tilde{\gamma}$, and thus

$$\overline{\boldsymbol{u}}_0 = \boldsymbol{u}_{\boldsymbol{V}}(z - \max \tilde{\gamma}) \text{ for all } z > \max \tilde{\gamma}, \tag{4.9}$$

where the Ekman flow $\boldsymbol{u}_{\boldsymbol{V}}$ is recalled in (3.6). In the limit of small wavelength, the roughness therefore behaves as a non-permeable wall. The flow does not enter the humps, and a classical Ekman layer forms above them. As a consequence, the dissipation satisfies

$$\mathscr{E} \to 1, \quad \lambda \to 0. \tag{4.10}$$

More information can be obtained on $\mathscr{E}$ at small λ, from higher-order correction terms of $\boldsymbol{u}_\lambda$. One can compute an expansion of the form

$$\left.\begin{aligned} \boldsymbol{u}_\lambda(\tilde{x}, z) &= \boldsymbol{u}_0(\tilde{x}, z) + \sum_{i \geqslant 1} \lambda^i \left(\boldsymbol{u}_i(\tilde{x}, z) + \boldsymbol{U}_i\left(\tilde{x}, \frac{z - \max \tilde{\gamma}}{\lambda}\right)\right), \\ p_\lambda(\tilde{x}, z) &= P_0\left(\tilde{x}, \frac{z - \max \tilde{\gamma}}{\lambda}\right) + \sum_{i \geqslant 1} \lambda^i \left(p_i(\tilde{x}, z) + P_i\left(\tilde{x}, \frac{z - \max \tilde{\gamma}}{\lambda}\right)\right), \end{aligned}\right\} \tag{4.11}$$

with two types of velocity profile: 'Ekman profiles' $\boldsymbol{u}_i$, similar to $\boldsymbol{u}_0$, and 'Shear layer profiles' (unaffected by rotation) $\boldsymbol{U}_i$, localized at the top of the humps. These shear layers vary over a typical height λ, and compensate for the discontinuity of the stress $\partial_z \boldsymbol{u}_{i-1}$ at the top of the roughness.

We sketch the construction of the first correction terms $\boldsymbol{U}_1$ and $\boldsymbol{u}_1$ only. From (4.6) and (4.9), one obtains

$$[\partial_z \boldsymbol{u}_0]|_{z = \max \tilde{\gamma}} = \boldsymbol{u}_{\boldsymbol{V}}'(0) \neq 0, \tag{4.12}$$

where the prime denotes a z derivative. A correction term is needed to balance this stress, namely $\lambda \boldsymbol{U}_1(\tilde{x}, (z - \max \tilde{\gamma})/\lambda)$. The profile $\boldsymbol{U}_1 = \boldsymbol{U}_1(\tilde{x}, \xi)$ is defined in the shear layer domain

$$\omega_{sl} = \{(\tilde{x}, \xi), 0 < \tilde{x} < 1, \xi \in \mathbb{R}\}, \tag{4.13}$$

https://doi.org/10.1017/S0022112006001856 Published online by Cambridge University Press

deduced from a vertical stretching of the hump. Injecting expansions (4.11) into (4.2), gives

$$(\partial_{\tilde{x}}, 0, \partial_\xi)P_0 - \Delta_{\tilde{x},\xi}\boldsymbol{U}_1 = 0, \quad \partial_{\tilde{x}}U_1 + \partial_\xi W_1 = 0. \tag{4.14a, b}$$

The lateral boundary conditions on $\boldsymbol{U}_1$ are

$$\left.\begin{aligned} &\boldsymbol{U}_1(0,\xi) = \boldsymbol{U}_1(1,\xi), \quad \xi > 0, \\ &\boldsymbol{U}_1(0,\xi) = \boldsymbol{U}_1(1,\xi) = 0, \quad \xi < 0, \end{aligned}\right\} \tag{4.15}$$

which correspond respectively to periodic boundary conditions above the humps, and solid boundary conditions inside the humps. As explained above, $\boldsymbol{U}_1$ should cancel the jump of $[\partial_z \boldsymbol{u}_0]$ at $z = \max \tilde{\gamma}$. Precisely, one can impose

$$[\boldsymbol{U}_1]\,|_{\xi=0} = 0, \qquad [\partial_\xi \boldsymbol{U}_1 + P_0 \boldsymbol{z}]|_{\xi=0} = -\boldsymbol{u}'_{\boldsymbol{V}}(0). \tag{4.16}$$

Equations (4.14), (4.15), (4.16) define the shear layer corrections $\boldsymbol{U}_1$. Note that V_1 is decoupled from (U_1, W_1); it satisfies a simple Laplace equation, whereas (U_1, W_1) satisfies a Stokes equation.

Similar elliptic equations with jump conditions have been considered in Jäger & Mikelic (2001), in the study of roughness-induced effects for Poiseuille flow. The crucial point is to understand the behaviour of $\boldsymbol{U}_1$ as $\xi \to \pm\infty$. One can easily show that

$$\nabla \boldsymbol{U}_1 \to 0 \quad \text{as } \xi \to \pm\infty. \tag{4.17}$$

From the no-slip condition (4.16) with $\xi < 0$, it follows that

$$\boldsymbol{U}_1 \to 0 \quad \text{as } \xi \to -\infty. \tag{4.18}$$

However, the same does not hold for $\xi \to +\infty$: due to the periodic boundary conditions, gradient control only provides

$$\boldsymbol{U}_1 - \overline{\boldsymbol{U}}_1 \to 0 \quad \text{as } \xi \to +\infty. \tag{4.19}$$

Yet the horizontal average satisfies

$$\overline{\boldsymbol{U}}_1 \to (\boldsymbol{V}_{sl}, 0) \quad \text{as } \xi \to +\infty, \tag{4.20}$$

for a non-zero velocity $\boldsymbol{V}_{sl}$. This is obtained after a few integrations. First, integration of the divergence-free condition over ω_{sl} yields

$$\lim_{\xi \to +\infty} \overline{W}_1 = 0. \tag{4.21}$$

Then, integrating (4.14a) with respect to $\tilde{x}$, for $\xi > 0$ yields $\partial_\xi^2(\overline{U}_1, \overline{V}_1) = 0$, which leads to

$$\boldsymbol{V}_{sl} = \lim_{\xi \to +\infty} (\overline{U}_1, \overline{V}_1) = (\overline{U}_1(\xi = 0), \overline{V}_1(\xi = 0)). \tag{4.22}$$

Finally, multiplying (4.14) by $\boldsymbol{U}_1$, and integrating by parts, one obtains, by relying on boundary and jump conditions (4.15) and (4.16),

$$\overline{U}_1(\xi = 0) = \frac{1}{u'_{\boldsymbol{V}}(0)} \int_{\omega_{sl}} |\nabla(U_1, W_1)|^2,$$

$$\overline{V}_1(\xi = 0) = \frac{1}{v'_{\boldsymbol{V}}(0)} \int_{\omega_{sl}} |\nabla V_1|^2,$$

https://doi.org/10.1017/S0022112006001856 Published online by Cambridge University Press

so that

$$\boldsymbol{V}_{sl} = \left(\frac{1}{u'_{\boldsymbol{V}}(0)} \int_{\omega_{sl}} |\nabla(U_1, W_1)|^2 , \frac{1}{v'_{\boldsymbol{V}}(0)} \int_{\omega_{sl}} |\nabla V_1|^2 \right) \neq 0. \tag{4.23}$$

We refer to Jäger & Mikelic (2001) for more details. Returning to the approximation $\boldsymbol{u}_\lambda \approx \boldsymbol{u}_0 + \lambda \boldsymbol{U}_1$, one needs an additional correction $\lambda \boldsymbol{u}_1$ to cancel the non-zero flow $\lambda \boldsymbol{V}_{sl}$ at infinity. The flow $\boldsymbol{u}_1$ is of the same type as $\boldsymbol{u}_0$, with $\boldsymbol{V}$ replaced by $-\boldsymbol{V}_{sl}$:

$$\left.\begin{aligned} \boldsymbol{u}_1 = \boldsymbol{0} \text{ for all } z < \max \tilde{\gamma}, \\ \boldsymbol{u}_1 = \boldsymbol{u}_{-\boldsymbol{V}_{sl}}(z - \max \tilde{\gamma}) \text{ for all } z > \max \tilde{\gamma}. \end{aligned}\right\} \tag{4.24}$$

Higher-order corrections could be derived following the same approach.

The computation of $\boldsymbol{U}_1$ and $\boldsymbol{u}_1$ casts useful light on how the dissipation $\mathscr{E}$ goes to 1 when λ tends to 0:

$$\mathscr{E}(\boldsymbol{V}) \approx 2 \int_{\tilde{\omega}} ((u_0, v_0) - \boldsymbol{V}) \cdot \boldsymbol{V}^\perp + 2\lambda \int_{\tilde{\omega}} (u_1, v_1) \cdot \boldsymbol{V}^\perp + 2\lambda^2 \int_{\tilde{x},\xi} (U_1, V_1) \cdot \boldsymbol{V}^\perp \tag{4.25a}$$

$$\approx 1 + 2\lambda \int_{\tilde{\omega}} (u_1, v_1) \cdot \boldsymbol{V}^\perp \tag{4.25b}$$

$$\approx 1 - 2\lambda (\boldsymbol{V}_{sl} + \boldsymbol{V}_{sl}^\perp) \cdot \boldsymbol{V}. \tag{4.25c}$$

Hence, the sign of $\left(\boldsymbol{V}_{sl} + \boldsymbol{V}_{sl}^\perp\right) \cdot \boldsymbol{V}$ determines whether $\mathscr{E}$ is less or more than unity for small enough λ. It depends on the direction of $\boldsymbol{V}$, and involves the solution of (4.14) and (4.15). Let us rewrite this solution as $\boldsymbol{U}_{\boldsymbol{V}} = (U_{\boldsymbol{V}}, V_{\boldsymbol{V}}, W_{\boldsymbol{V}})$. When $\boldsymbol{V} = (\cos(\varphi), \sin(\varphi))$, the Ekman flow satisfies

$$u'_{\boldsymbol{V}}(0) = \sqrt{2}\, \cos(\varphi + \pi/4), \quad v'_{\boldsymbol{V}}(0) = \sqrt{2}\, \sin(\varphi + \pi/4). \tag{4.26}$$

In particular, $u'_{(1,0)}(0) = 1$, $v'_{(1,0)}(0) = 1$. The linearity of (4.14) and (4.15) then provides

$$(U_{\boldsymbol{V}}, W_{\boldsymbol{V}}) = \sqrt{2} \cos(\varphi + \pi/4) \big(U_{(1,0)}, W_{(1,0)}\big), \quad V_{\boldsymbol{V}} = \sqrt{2} \sin(\varphi + \pi/4) V_{(1,0)}. \tag{4.27}$$

Together with (4.23), this yields

$$-(\boldsymbol{V}_{sl} + \boldsymbol{V}_{sl}^\perp) \cdot \boldsymbol{V} = 2 \cos(\varphi + \pi/4) \cos(\varphi - \pi/4) \left(\int \big|\nabla V_{(1,0)}\big|^2 - \int \big|\nabla \big(U_{(1,0)}, W_{(1,0)}\big)\big|^2 \right). \tag{4.28}$$

In particular, when $\boldsymbol{V} = (1, 0)$

$$-(\boldsymbol{V}_{sl} + \boldsymbol{V}_{sl}^\perp) \cdot \boldsymbol{V} = \int \big|\nabla V_{(1,0)}\big|^2 - \int \big|\nabla \big(U_{(1,0)}, W_{(1,0)}\big)\big|^2. \tag{4.29}$$

This quantity can easily be estimated numerically: finite-element simulation yields

$$\int \big|\nabla V_{(1,0)}\big|^2 - \int \big|\nabla \big(U_{(1,0)}, W_{(1,0)}\big)\big|^2 \approx 0.4. \tag{4.30}$$

On the other hand, when $\boldsymbol{V} = (0, 1)$

$$-(\boldsymbol{V}_{sl} + \boldsymbol{V}_{sl}^\perp) \cdot \boldsymbol{V} = -\int \big|\nabla V_{(1,0)}\big|^2 + \int \big|\nabla \big(U_{(1,0)}, W_{(1,0)}\big)\big|^2 < 0. \tag{4.31}$$

For general angles φ, the correction to the dissipation remains bounded by the two extreme values $\pm(\int |\nabla V_{(1,0)}|^2 - \int |\nabla (U_{(1,0)}, W_{(1,0)})|^2)$.

https://doi.org/10.1017/S0022112006001856 Published online by Cambridge University Press

One can draw two conclusions based on this small wavelength argument:

1. The dissipation is determined by the orientation of $\boldsymbol{V}$ *with respect to the roughness* (*i.e. to* $\boldsymbol{e}_x = (1.0)$). In other words, the extreme behaviour of the dissipation is obtained for $\boldsymbol{V}$ parallel to $(1, 0)$ ($\varphi = 0$) and $\boldsymbol{V}$ orthogonal to $(1, 0)$ ($\varphi = \pi/2$).

2. When $\boldsymbol{V}$ *is parallel to* $(1, 0)$*, the dissipation is strictly more than 1. On the other hand, when* $\boldsymbol{V}$ *is orthogonal to* $(1, 0)$*, the dissipation is stricly less than one.*

Note that these results are compatible with those derived from the small-amplitude analysis. They will be interpreted from a physical point of view in § 5.

5. Numerical solutions and global physical interpretation

5.1. *Numerical computations*

We discuss here the numerical simulations of system (2.40). Computations are carried out in a finite domain, checking that the solutions obtained are independent of the domain height. Since p vanishes as $z \to \infty$, it is set to zero at the top of the computational box. The computations have been performed using *Femlab*, finite-element software, and have been validated with *Freefem*, a freeware finite-element package.

We consider sinusoidal boundaries of the type

$$\partial\omega = \left\{(x, z),\, z = \alpha \sin\left(\frac{2\pi}{\lambda}x\right)\right\}, \tag{5.1}$$

for various parameters α and λ. Special attention has been paid to the variation of the dissipation $\mathscr{E}(\boldsymbol{V})$ with respect to α, λ and the flow at infinity $\boldsymbol{V} = (\cos(\varphi), \sin(\varphi))$.

The problem under investigation being linear, it is not necessary to compute the dissipation for the whole range of angles φ. Instead the dependence of the dissipation on the angle φ can be made explicit, provided only three quantities are estimated. One can write

$$\mathscr{E}(\boldsymbol{V}(\varphi)) = \mathscr{E}_0 \cos^2(\varphi) + \mathscr{E}_1 \sin^2(\varphi) + \mathscr{E}_2 \cos(\varphi)\sin(\varphi), \tag{5.2a}$$

where

$$\mathscr{E}_0 = \mathscr{E}(\boldsymbol{V}(\varphi = 0)) = \int |\nabla \boldsymbol{u}_0|^2, \qquad \mathscr{E}_1 = \mathscr{E}(\boldsymbol{V}(\varphi = \pi/2)) = \int \left|\nabla \boldsymbol{u}_{\pi/2}\right|^2, \tag{5.2b}$$

$$\mathscr{E}_2 = \int \nabla \boldsymbol{u}_0 \cdot \nabla \boldsymbol{u}_{\pi/2}. \tag{5.2c}$$

In all the computations we have carried out, the third term $\mathscr{E}_2$ was negligable compared to the two other terms $\mathscr{E}_0$ and $\mathscr{E}_1$. For this reason, we focus our investigation on the two cases $\varphi = 0$ and $\varphi = \pi/2$.

The outputs of the numerical simulations can be compared with the analytical results of the previous sections. Various curves of $\mathscr{E}_0$ and $\mathscr{E}_1$ are shown in figure 3, in the extreme cases $\varphi = 0$ and $\varphi = \pi/2$. They exhibit typical features that were pointed out in § 3 and § 4. For instance, $\mathscr{E}_0$ is always larger than in the flat case. Note that the dissipation increases rapidly with the amplitude α of the roughness. When α increases by a factor about 3 (from 2.1 to 6.1), the maximum dissipation increases by a factor 10. This highlights that the quantitative behaviour relevant to the classical Ekman theory no longer holds with wavy boundaries. When $\varphi = \pi/2$, the dissipation can be either larger or smaller than 1, depending on the wavelength λ.

When $\alpha \to 0$, the numerical quantities converge to those obtained in the asymptotic analysis. The analytical expression (3.17) can be estimated in the special case of a

https://doi.org/10.1017/S0022112006001856 Published online by Cambridge University Press

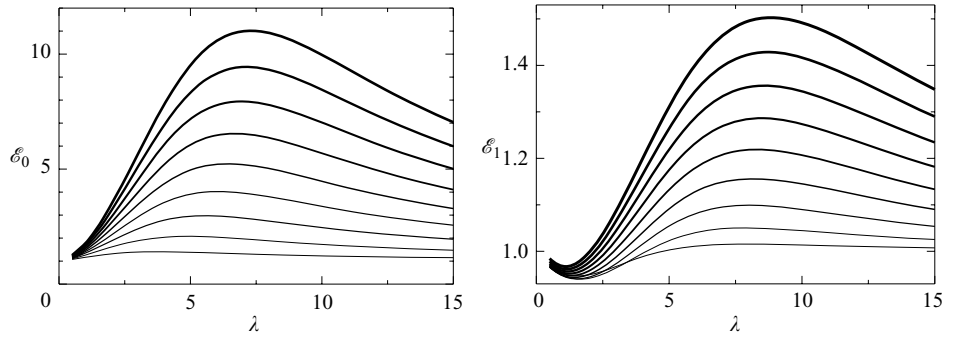


FIGURE 3. $\mathscr{E}_0$ and $\mathscr{E}_1$ *vs.* λ. The dissipations associated with the numerical solutions of the governing equations (2.40) are shown for α ranging from 2.1 to 6.1 with steps of 0.5 by continuous lines of increasing solidity.

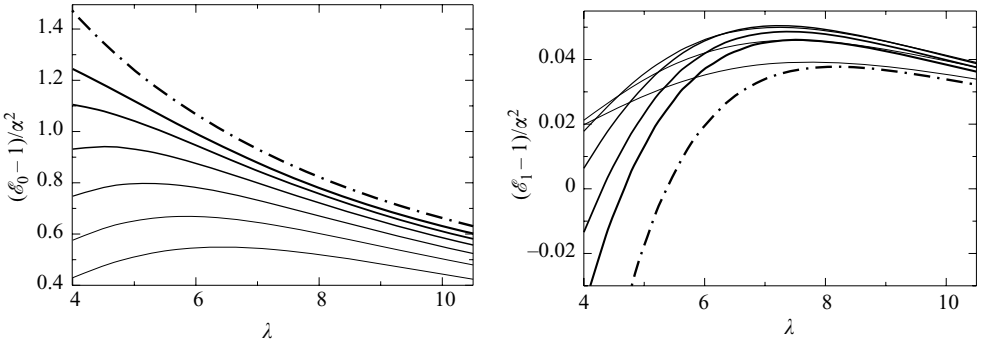


FIGURE 4. $(\mathscr{E}_0-1)/\alpha^2$ and $(\mathscr{E}_1-1)/\alpha^2$ *vs.* λ. The dissipations associated with the numerical solutions of the governing equations (2.40) are shown for α ranging from 3.03 to 0.4 with a geometric progression of ratio 2/3 by continuous lines of increasing thickness; the dissipations provided by the asymptotic equation (3.17) are identified by the dot-dashed curves. The smaller the value of α, the closer the curve is to the asymptote.

sinusoidal boundary. It then matches remarkably well the finite element computations performed at low values of α. This is illustrated in figure 4, in which $(\mathscr{E}_0-1)/\alpha^2$ and $(\mathscr{E}_1-1)/\alpha^2$ are plotted as a function of wavelength λ, for various small amplitudes. Theoretical and numerical approaches are found to be in excellent agreement.

When $\lambda \to 0$, one can verify several features described in the asymptotic expansion. First, for small enough values of λ, a plain Ekman layer forms above the humps (see figure 5). Moreover, as λ increases from zero, it is clear from figure 3 that $\mathscr{E}_0$ increases, whereas $\mathscr{E}_1$ decreases, as expected from the asymptotic description of § 4.

5.2. *Physical interpretation*

A physical description of the above results must capture the evolution of the dissipation $\mathscr{E}$ both with λ and with the angle φ, as depicted on figure 3.

A clear characteristic of these graphs is that behaviour depends very strongly on whether $\boldsymbol{V}$ is oriented along the roughness (i.e. $\varphi = \pi/2$) or across the roughness (i.e. $\varphi = 0$).

When $\lambda \to +\infty$, the horizontal variations of the boundary are infinitesimal, so that it behaves locally as a flat horizontal wall. As a consequence, as observed in the

https://doi.org/10.1017/S0022112006001856 Published online by Cambridge University Press

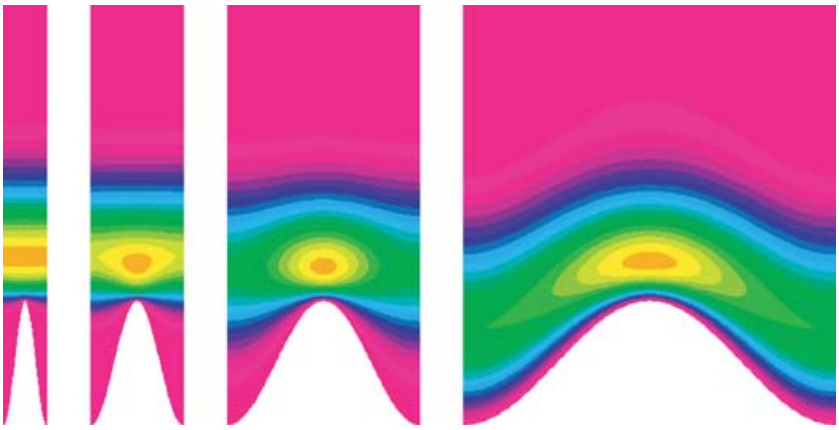


FIGURE 5. Detachment of the boundary layer for sufficiently small values of λ. Streamwise component of the velocity u for $\varphi = 0$, $\alpha = 1$, and $\lambda = 0.7, 1.5, 3.1, 6$. The computational domain extends to higher z but has been truncated for clarity of representation. The colour code ranges between -0.35 (orange) and 3×10^{-2} (red).

graphs, both

$$\mathscr{E}_0, \mathscr{E}_1 \to 1, \quad \lambda \to +\infty. \tag{5.3}$$

For smaller values of λ, the horizontal variations can no longer be neglected, and the slope effects play an increasingly important role. The effect on the rotating flow differs according to the value of φ (here $\varphi = 0$ or $\varphi = \pi/2$). For very large λ and any point $x_0, z_0 = \alpha \sin(2\pi/\lambda\, x_0)$ on the boundary, the wavy shape of the boundary near x_0, z_0 is approximated well by

$$z \approx z_0 + \cos\left(\frac{2\pi}{\lambda} x_0\right) \frac{2\pi}{\lambda}(x - x_0). \tag{5.4}$$

In other words, in this regime the boundary can be interpreted locally as an inclined planar boundary.

On the one hand, when $\varphi = 0$, the flow at infinity goes transversally to the boundary. Hence, the fluid must deviate drastically when approaching the boundary. This creates strong vorticity, and thus friction. Therefore, the quantity $\mathscr{E}(V)$ increases strongly as λ decreases. When $\varphi = \pi/2$, on the other hand, this situation does not hold, since the flow at infinity is oriented tangentially to the wall. Such a configuration (Ekman flow near a slope) is very well described by Pedlosky (1979). It is well-known that the Ekman pumping, and so the friction, is larger then than in the horizontal case, because of the increase in the effective Ekman number as E is replaced by $E/\cos(\theta)$. The quantity $\mathscr{E}(V)$ therefore also increases as λ decreases, but the effect is much less pronounced than in the case $\varphi = 0$.

As λ continues to diminish, the above localy planar approximation no longer holds, curvature becomes important and the boundary becomes significantly hollowed. In these gutter-like structures, the orientation of the flow is forced to be mainly along $(0, 1)$, tangential to the boundaries of the hollows. When $\varphi = 0$, it amplifies the deflection of the flow with depth characterizing the Ekman spiral. As a consequence, the dissipation $\mathscr{E}(V)$ continues to increase. On the other hand, when $\varphi = \pi/2$, the spiralling tends to be reduced by this effect; the dissipation $\mathscr{E}(V)$ thus decreases. The gutter-like structure associated with our two-dimensional boundaries therefore tends

https://doi.org/10.1017/S0022112006001856 Published online by Cambridge University Press

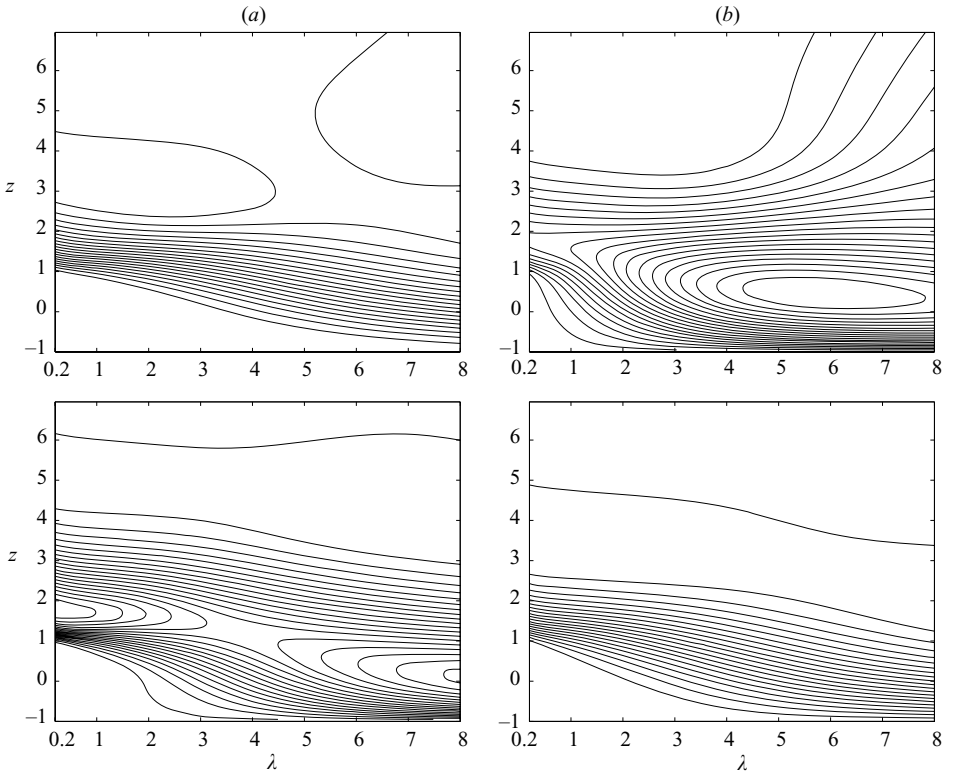


FIGURE 6. Cross-sections at $x = 3\lambda/4$ for $\gamma(x) = \sin(2\pi x/\lambda)$ (corresponding to the boundary minimum) for varying λ. Isovalues of (*a*) u and (*b*) v in the (λ, z)-plane. The top line corresponds to $\varphi = 0$, the bottom line to $\varphi = \pi/2$. The boundary layer expulsion at small λ is clear from these graphs.

to orientate the flow, respectively strengthening or reducing the flow $\boldsymbol{u}^{\perp}$ orthogonal to the mainstream $\boldsymbol{V}$, depending on the relative orientation of the mainstream to the roughness, respectively transverse or tangential.

The evolution just described holds as long as λ is large enough. For smaller values of λ, a new phenomenon occurs: the boundary layer detaches from walls of large curvatures. This detachment should not be confused with nonlinear detachments in the framework of Prandtl layers, since it does not involve the same physical ingredients. This phenomenon is exemplified well in figures 5 and 6. In the limit $\lambda = 0$, the layer develops outside the hollows, as was already deduced mathematically in § 4. This suppression of motion inside the narrow humps can be understood by considering the local effective Reynolds number in these regions: $|V|\lambda$. This number decreases with λ, hence motion eventually vanishes inside the hollows.

Owing to this detachment of the boundary layer, the constraints imposed by the boundary of the hollows on the flow get weaker in the small-λ limit. As a result $\mathscr{E}(\boldsymbol{V})$ decreases for $\varphi = 0$, whereas it increases back to unity for $\varphi = \pi/2$.

6. Concluding remarks

The investigation of Ekman layers near wavy boundaries offers an unexpected variety of effects. We have only considered smooth and periodic boundary profiles

https://doi.org/10.1017/S0022112006001856 Published online by Cambridge University Press

in this work. Sharp structures (such as sawtooth) could yield more complicated behaviour. The rotation axis was taken as normal to the large-scale boundary (equivalent to the poles on a sphere like the Earth); new effects could be expected if the axis were slanted with respect to the boundary normal. In addition, only linear problems have been considered here. It well known that nonlinearities can trigger Ekman layers instabilities which are not trivial even in the planar case. Next to a wavy boundary nonlinearities can strongly affect the solution even before the layer itself becomes unstable. We delay such investigations to future studies.

We wish to thank Professor Emmanuel Grenier and more generally participants in the ACI program "Aspects mathématiques de la géodynamo" for discussions at preliminary stages of this work. We are grateful to Daniel Nethery for help with the manuscript revision.

REFERENCES

Bell, P. I. & Soward, A. M. 1996 The influence of surface topography on rotating convection. *J. Fluid Mech.* **313**, 147–180.

Dormy, E., Roberts, P. H. & Soward, A. 2005 Boundary layers in the core. In *Encylopedia of Geomagnetism* (ed. D. Gubbins). Springer (in press).

Ekman, V. W. 1905 On the influence of the earth's rotation on ocean currents. *Ark. Mat. Astr. Fys.* **2**, no. 11.

Gérard-Varet, D. 2003 Highly rotating fluids in rough domains. *J. Maths Pures Appl.* **82**, 1453–1498.

Greenspan, H. P. 1968 *The Theory of Rotating Fluids.* Cambridge University Press.

Jäger, W. & Mikelic, A. 2001 On the roughness-induced effective boundary conditions for an incompressible viscous flow. *J. Diffl Equat.* **170**, 1.

Kunze, E. & Llewellyn Smith, S. G. 2004 The role of small-scale topography in turbulent mixing of the global ocean. *Oceanography* **17**, 1.

Narteau, C., Le Mouël, J.-L., Poirier, J. P., Sepulveda, E. & Shnirman, M. 2001 On small-scale roughness of the core mantle boundary. *Earth Planet. Sci. Lett.* **191**, 49–60.

Pedlosky, J. 1979 *Geophysical Fluid Dynamics.* Springer.

Ponty, Y., Gilbert, A. D. & Soward, A. M. 2001 Kinematic dynamo action in flows driven by shear and convection. *J. Fluid Mech.* **435**, 261–287.

Vanneste, J. 2000 Enhanced dissipation for quasi-geostrophic motion over small-scale topography. *J. Fluid Mech.* **407** 105–122.

https://doi.org/10.1017/S0022112006001856 Published online by Cambridge University Press